Theoretical and Practical Considerations of Spatially Offset Raman Spectroscopy (SORS) and Micro-SORS

Lux A, Conti C, Botteon A, Mosca S, Matousek P.

Published version information

Citation: Lux A, Conti C, Botteon A, Mosca S, Matousek P. Theoretical and Practical Considerations of Spatially Offset Raman Spectroscopy (SORS) and Micro-SORS. Applied Spectroscopy. 2024;0(0).

DOI: doi:10.1177/00037028241270263

Theoretical and Practical Considerations of Spatially Offset Raman Spectroscopy (SORS) and Micro-SORS

A. Lux[1,2,3*], C. Conti[1], A. Botteon[1], S. Mosca[3], P. Matousek[1,3*]

[1] *Institute of Heritage Science, National Research Council (CNR-ISPC), Via Cozzi 53, 20125, Milan, Italy.*

[2] *Sapienza University of Rome, Faculty of Literature, Department of Classics, Piazzale Aldo Moro 5, 00185, Rome, Italy.*

[3] *Central Laser Facility, Research Complex at Harwell, STFC Rutherford Appleton Laboratory, Harwell Campus, OX11 0QX, United Kingdom.*

Abstract

Spatially Offset Raman Spectroscopy (SORS) is typically used to non-invasively investigate stratified samples that possess features on a millimetre scale, whereas micro-SORS usually deals with micrometre thick layered samples: however, there are many instances where these boundaries are intertwined, sometimes indicating the possibility of using both techniques as well as circumstances that present mutual exclusion to their applicability. The aim of this study is to establish an application protocol providing better insight into their suitability for deployment in various scenarios. The differences and similarities between the two approaches are investigated highlighting their strengths and limitations considering both theoretical and practical aspects. Diverse available parameters entail prospects and restrictions of both the techniques and give rise to specific instrumental effects: namely, the overlap between the collection and excitation areas, the percentage of collected area for a given spatial offset and the accuracy in the definition of the spatial offset (spread effect). These aspects are studied and exemplified on mock up samples relevant to the field of cultural heritage. The samples are characterized by high compositional complexity comprising features ranging from micrometre to millimetre scales. The conclusions reached are also relevant to other scientific areas such as biomedical, forensic or energy harvest ones.

Introduction

Non-invasive probing of the subsurface of materials with high chemical specificity is a topical and fast evolving area of analytical sciences. In this context, Spatially Offset Raman Spectroscopy (SORS) has shown great promise in many such applications, being able to satisfy multiple requirements (e.g. non-invasiveness and non-destructiveness, high chemical selectivity and portability)[1]. In case of turbid materials, the technique is able to retrieve signals from the subsurface thanks to the separation between the illumination and collection zones: in essence, Raman photons generated deeper in the sample are statistically more likely to travel sideways further through the sample than surface photons, allowing the investigation of inner layers[2]. In a SORS measurement a series of spectra can be obtained, each with a certain spatial offset (Δs) from the illumination zone. As the offset increases, the overall intensity of the corresponding spectrum decreases, since less Raman photons can be detected overall: however, in the case of a two-layer sample the signal originating from the top layer will decay more rapidly than the signal originating from the bottom one. For example, by simply normalizing all the series to a Raman band representative of the bottom layer, it is possible to visualise the relative decay of the top layer band. Moreover, a sublayer spectrum can be isolated by subtracting a zero spatial offset spectrum from a non-zero one with a scaling factor set to cancel Raman features belonging to the surface layer[Error! Bookmark not defined.]. In some other cases, the surface contribution entirely disappears in the collected SORS spectra, leading to a complete separation between the top and bottom layer signals and so to the representative probing of the subsurface of the sample, with no need for subtraction.

Micro-SORS is a variant of SORS proposed by Conti *et al*[4]. employing microscope objectives in both the excitation and collection paths, to enable probing micrometric thick layers. Since then, several studies[5,6] have been carried out demonstrating its potential in many applications, especially in the cultural heritage field. In general, micro-SORS and SORS together have a potential to investigate samples that possess layers with thicknesses ranging from tens of micrometres to millimetres[7] and even centimetres[8–10] across diverse range of fields. The techniques are relatively new and one key aspect not fully addressed to date is how they differ from each other in their performance and which aspects one needs to take into consideration when selecting a specific approach to a particular sample and problem at hand. This study focusses on addressing these points. These are particularly important at the boundaries between the two techniques when probing layers on the scale of several hundred micrometres to millimetres in order to understand which approach is the most suitable. In this paper, we aim to show the differences between the performances of the two methods and emphasize key characteristics that set them apart aiding one to establish an optimum procedure for any specific practical application and subsequent data analysis and data interpretation. Although in this study we used samples mimicking cultural heritage situations, the findings are generally extendable by analogy to other analytical areas (for example, to biomedical[9,11], aerospace, food science[12] or solar energy generation[13,14]).

Experimental

The SORS instrument used here was custom-made and is described in detail elsewhere[15]. It is based around a point-like excitation and collection configuration. The excitation optical path utilizes an 829.40 nm excitation wavelength, two bandpass filters (LL01-830-25, Semrock Inc.) a quarter waveplate (WPQ05M-830, Thorlabs) converting the linearly polarized laser beam into circularly polarized beam and a 100 mm focal lens to relay the laser to ~500 µm diameter spot at sample surface. The backscattered Raman radiation is collected from a zone of ~1.5 mm diameter at a ~35° angle to the normal incidence using a telescope system made of two 50 mm lenses, two long-pass filters and an optical fibre bundle (custom-made round to linear, CeramOptec Industries, Inc.). The collected light is coupled to a spectrometer (HoloSpec f/1.8i, Kaiser Optical Systems) with a CCD (DU420A-BR- DD-9UW, Andor Technology). The SORS spatial offset is set by moving the entire collection path assembly along the plane parallel to the sample surface with a motorized stage (MTS25-Z8 with KDC101 controller, Thorlabs) in a range of spatial offsets of 0 to 11 mm (see Fig S1a). SORS measurements have been acquired with 7 different offsets (namely: 0, 0.5, 1, 2, 3, 4 and 5 mm offsets) even though not all of them have been always used since, especially for larger offsets, some did not yield any additional information. The employed power was about 55 mW at sample and the overall acquisition time was 60 s (6 s acquisitions with 10 repeats).

The micro-SORS instrument, shown in Figure S1b, is a Renishaw InVia Qontor device specifically designed for micro-SORS measurements. Concerning the excitation path, the instrument is equipped with an external laser arm mounted on an SB 100 micrometric stage for setting spatial offsets. A Mitutoyo super-long working distance (SLWD – 30.5 mm) 20X objective with M25 adaptor is used, positioned at ~38° with respect to the normal to the incidence plane and connected to the laser (Renishaw HPNIR with 785 nm wavelength) by a 50 µm diameter core optical fibre. Raman photons are collected with a standard optical path, using N-PLAN 20X (NA 0.35 – WD 6.9) objective. The dimensions of the collection and excitation spots were evaluated using a simple approach, described in the Instrumental Considerations section. The employed CCD is a Renishaw CTX-1024A256-FDU Peltier cooled (-70 °C) NIR enhanced CCD camera, with a pixel dimension of 26x26 µm. The spectral resolution is 1–2 cm^{-1}. The overall acquisition time and the collected offset steps were set identical to SORS measurements: the employed power, however, was 100 mW.

All micro-SORS spectra were acquired with WiRe software, and both SORS and micro-SORS spectra were externally processed using OPUS (Bruker) software.

Samples

The samples were selected to highlight the instrumental differences and specifics of SORS and micro-SORS approaches as well as to illustrate techniques' limitations. These were assembled to have different thicknesses of the top layer in order to mimic different scenarios one can encounter in cultural heritage. The samples were of increasing complexity. The first three sample types (S1-S3) are homogeneous, whereas the last one (S4) is heterogeneous in terms of the thickness of its top layer. The former ones were employed to demonstrate the practical differences between SORS and micro-SORS methods with increasing complexity, and the latter was chosen to show their different responses when presented with non-uniform thickness of the top layer. Moreover, S4 set of samples differs from the others since it possesses only a single top layer thickness but of differing compositions (10%, 20% and 30% ratio between the amount of gypsum and calcite). The samples are described in Table 1.

Table 1. Samples used in the study.

Sample label	**S1**	**S2**	**S3**	**S4**
Mock-up of	Standard sample	Painted stratigraphy	Limewash	Salts diffusion
Substrate	Polytetrafluoroethylene (PTFE)	Phthalocyanine blue pigment ($C_{32}H_{16}N_8Cu$) mixed in acrylic media	Carrara marble ($CaCO_3$)	Calcite powder ($CaCO_3$) mixed with PVA
Top layer	Polystyrene (PS)	Red ochre pigment (mainly haematite—Fe_2O_3) and calcite ($CaCO_3$) mixed in acrylic media	Gypsum ($CaSO_4 \cdot 2H_2O$)	Gypsum and calcite powders mixed with PVA
Top layer thickness (mm)	0.05, 0.1, 0.25, 0.5, 1, 2, 3, 4, 5	0.15, 0.3, 0.5, 1, 2, 3, 4, 5	0.5, 1, 2, 3, 4, 5	1 ± 0.5 mm
Top layer composition	Constant	Constant	Constant	Varied - 10%, 20% and 30% gypsum/calcite fractions

The preparation of the samples was carried out manually.

- S1 was selected as a standard sample composed of polytetrafluoroethylene (PTFE) and polystyrene (PS). In cultural heritage, superimposed layers of polymers can be found in contemporary art and in product design. The thinnest layers of PTFE were obtained by single or stacked layers of PTFE tape, which was 50 µm thick.S2 mimics a painted stratigraphy composed of

two layers. The phthalocyanine blue substrate was prepared by pouring liquid paint into a small round plastic cast (diameter around 5 cm) and left to dry on a laboratory bench for a couple of days. Filler material was periodically added to compensate the shrinking due to the drying process in order to avoid the formation of cavities. The red ochre top layers were prepared similarly, so by pouring liquid paint into a small round plastic cast: the obtained block was then cut with a precision cutter into thin layers of diverse thicknesses (0.5, 1, 2, 3, 4, 5 mm)

- The gypsum top layers of S3 were prepared similarly starting from a solid block of quick setting gypsum (Rapid Mix, scagliola) that had been previously mixed with water to consolidate. Once again, it was then cut with a precision cutter into the desired layers (0.5, 1, 2, 3, 4, 5 mm thick); S3 simulates a gypsum limewash applied over a marble substrate, obtained from a storage facility at ISPC laboratory.
- S4 simulates the diffusion of soluble salts inside plasters and mortars, a typical decay mechanism in historical buildings. Mixtures of calcite (CAS: 471-34-1, VWR Chemicals), the main mineral of many plasters and mortars, and gypsum, a very common soluble salt (in this case, the same gypsum employed before), were prepared by mixing the raw powders with Vinavil (PVA, polyvinyl alcohol). Different ratios between the amount of gypsum (salt) and calcite (matrix) powders were considered, namely:
    - composition 1 - 10% of gypsum in calcite matrix
    - composition 2 - 20% of gypsum in calcite matrix
    - composition 3 - 30% of gypsum in calcite matrix

  The preparation consisted of manually weighing and mixing the powders, then adding the necessary amount of PVA to render the substance pourable. A final step consisted of placing these into an oven at around 50-60 °C for drying. Afterwards, all the blocks were cut with a precision rotating blade cutter to obtain layers of different thicknesses. It is worth mentioning that the samples were rather hard and resilient to the cutting blade and small thicknesses were challenging to obtain. Consequently, the top layer thickness was uneven with an average error of thickness of $\pm$ 0.5 mm, and the selected usable thickness depended on the quality of the cut.

Instrumental considerations

It is important to point out key differences between the SORS and micro-SORS techniques. These mainly stem from the vast differences in the spatial scales of their collection and illumination configurations. As the excitation area is much smaller for micro-SORS, the Raman signal decreases for the top layer as the spatial offset increases in a much steeper manner for micro-SORS rather than SORS. Moreover, SORS geometry involves the illumination of a greater portion of the sample as well as the collection of Raman signals from a much larger area. This leads to a greater ability by SORS to average sample heterogeneity, at the expense of a lower spatial resolution and in the collection of a greater fraction of available signal on a sample surface. On the other hand, micro-SORS can provide much higher contrast between layers since the collection areas are better separated. In turn, considering the illumination side, micro-SORS possesses typically a higher risk of potential sample damage due to much higher laser intensity present at the sample surface.

Overall, there are several key parameters to consider when comparing SORS and micro-SORS:

- the overlap area between the collection and excitation spots;
- the fraction of the available signal area on sample surface from which signal is collected for a given spatial offset;
- how well the spatial offset is defined for any specific configuration (i.e. the blurring of spatial offsets).

We discuss these effects in turn in the following sections.

Overlap Effect

Since the illumination and collection areas can be, in the simplest representation, modelled as circles, the overlap effect can be easily visualized as an intersection between these: initially, when the offset is zero (conventional Raman spectrum), the circles are centred onto one another, and then they start being separated as spatial offset increases. If the circles have the same diameter, as soon as the distance between their centres becomes greater than zero the overlap area would become a fraction of the initial value. However, for our SORS instrument the illumination disk is much smaller than the collection area (the illumination area is 9 times smaller) and so for certain smaller offsets the excitation disk is fully contained within the collection circle. The consequence of the overlap is that it provides, in part, signal also from the zero spatial offset even when the spatial separation between the collection and illumination areas (defined as separation between their centres) is non zero. Thus, this sort of contamination impacts achievable measurement contrast between the surface and subsurface layers.

In order to explain the regime where the excitation area is not fully contained within collection zone anymore, we have employed the following formula[16] that gives the overlap area between two circles of different radii as a function of the distance between their centres:

$$A_{overlap} = R^2 \cos^{-1}\left(\frac{d^2 + R^2 - r^2}{2dR}\right) + r^2 \cos^{-1}\left(\frac{d^2 - R^2 + r^2}{2dr}\right) - \frac{1}{2}\sqrt{(-d + R + r)(d + R - r)(d - R + r)(d + R + r)} \qquad (1)$$

where R, r are the radii of the collection and excitation spots respectively $(R > r)$ and d is the distance between the centres of the circles (see Figure 3a). The formula has limiting conditions outside of which it is not valid anymore:

- when $d \leq R - r$, when the smaller circle is completely contained within the larger one, and $A_{overlap} = \pi r^2$;
- when $d \geq R + r$, i.e. when there is no overlap anymore, which means $A_{overlap} = 0$.

As mentioned above, for smaller offsets (i.e. 'd'), the optical geometry can lead to an overlap of the collection and excitation areas. For SORS, in our specific case, up to 0.5 mm offset ($d \leq R - r = 0.5\ mm$) the laser spot is fully contained within the collection, and then the overlap area diminishes following equation (1) until its limiting condition ($d \geq R + r = 1\ mm$).

This model can also be useful to measure estimated dimensions of the collection and excitation spot sizes. We employed this approach to estimate these parameters for the micro-SORS instrument. Silicon was chosen as a standard sample for this test, as it is highly absorbing material (absorption coefficient[17,18] at 785 nm is approximately $10^3\ cm^{-1}$, which gives a rough estimate of maximum Raman probed depth to be around 10 µm). As such, the Raman signal originates only from a very thin top layer of the sample. In the experiments, whilst the collection area remained fixed, the laser beam was moved on sample surface from 0 to a 140 µm with a 1 µm step, starting from outside the collection zone (no Raman signal) and crossing it until the collected signal disappeared again. Plotting the reference Raman band of silicon versus the spatial displacement of the laser yielded a curve shown in Figure 1b (only a half of the curve is shown): under the assumption of uniform intensity of the laser beam across the illumination zone, for illumination and collection circles of different diameters the extent of the slope indicates the size of the smaller circle whereas the width of the plateau indicates the dimension of the greater one. The result of the measurement were satisfactorily modelled with spot diameters of 27.5 µm and 16 µm (see Fig.1c). Slight discrepancies between the

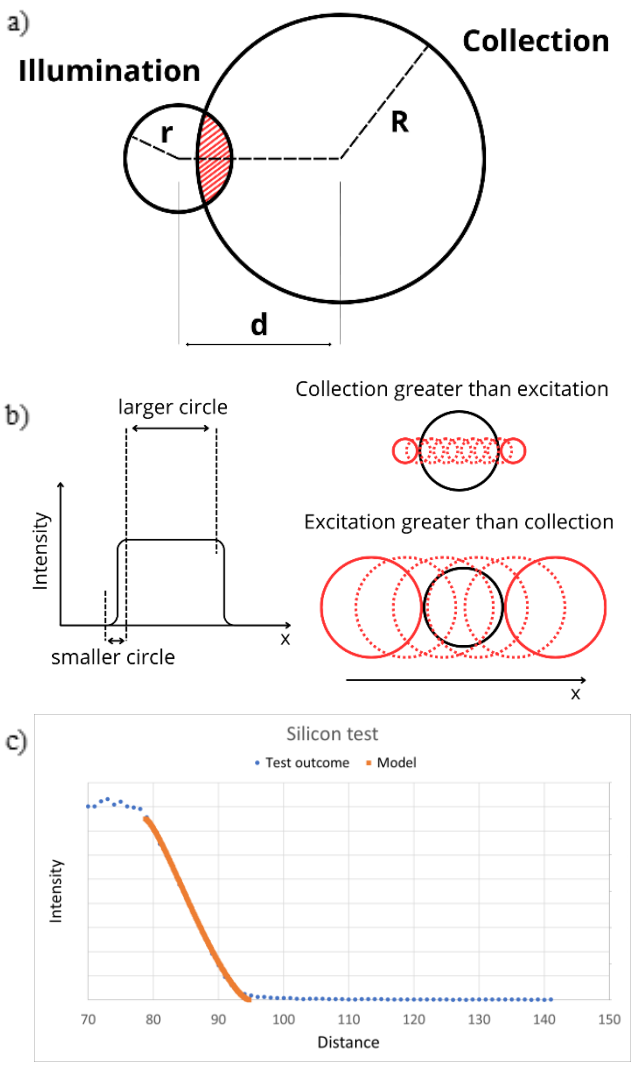

Figure 1. a) Schematics of the overlap of excitation and collection spots. The distance d corresponds to the spatial offset previously defined; b) schematics of the method to estimate collection and excitation spot sizes exploiting the overlap effect; c) comparison with the obtained results and the model.

theoretical calculations and experimental observables are attributed to the approximations used in our model – e.g. in reality we are probing a sample volume rather than an infinitely thin layer (which means that it is an effective estimation of the spot sizes within ~10 μm of the sample depth, rather than just at the sample surface), the consideration of circle instead of an ellipse on the laser side, which would be more accurate for the excitation spot or the consideration of perfect focusing of both the collection and excitation and assuming the uniform illumination across the illumination zone. By observing the approximate dimension of the laser beam using a Raman microscope visual camera (Figure S4), the larger of the two circles was assigned to the laser beam spot size.

Overall, it is noted that the overlap phenomena are confined to much smaller spatial range of offsets for micro-SORS, since the difference between the excitation and collection spots radii is much smaller compared to SORS one. Therefore, as it can be seen from Figure 2a where the fraction of the overlap area is shown $\left(\frac{A_{overlap}}{A_{excitaion}}\right)$, the overlap effect for micro-SORS disappears already above ~20 μm offset, in our case, providing an improved contrast between surface and subsurface signals; in contrast, for our experimental parameters the overlap for SORS endures up to 1 mm spatial offset, leading to greater "contamination" of the surface Raman signal with the subsurface signal.

The schematics in Figure 2b,c highlights how the micro-SORS results typically in a more well-defined Δs and therefore yielding a higher contrast of signals between the top and bottom layers, even for Δs below 1 mm. As such, when the layers to be analysed are on a micrometre scale, micro-SORS would naturally be a better suited technique.

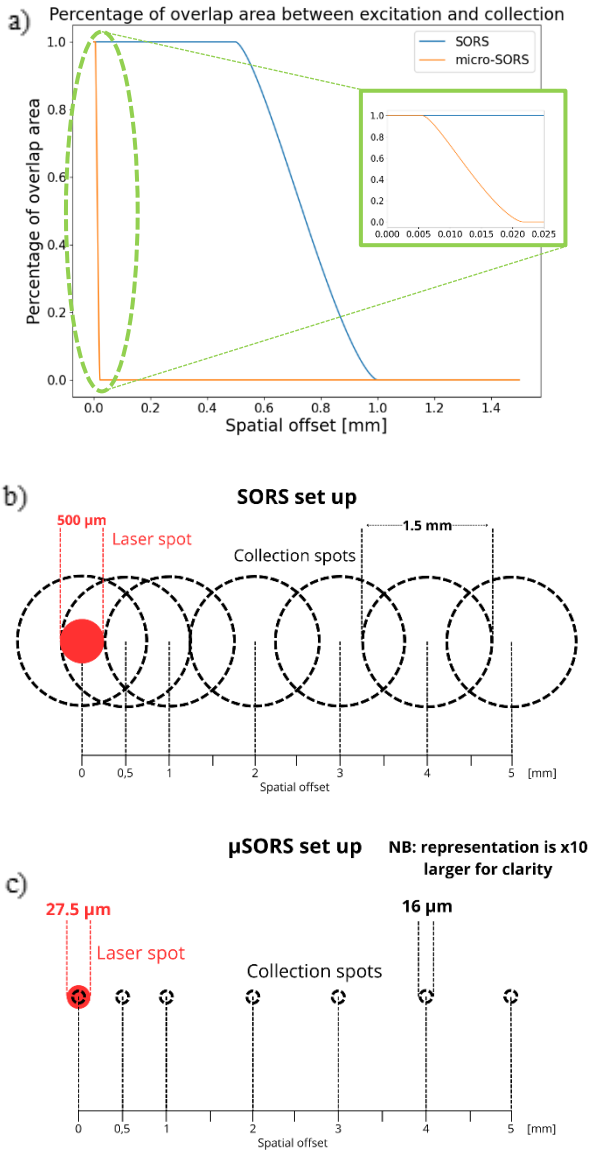

Figure 2. a) Fraction of overlap area between excitation and collection spots for both techniques; b) schematics of the SORS set-up, with the dimension of the excited and collected areas underlined; b) corresponding schematics for micro-SORS.

Collection Area Effects

Another important differentiating feature to consider is the percentage of the collected area on sample surface, for a given spatial offset around the illumination zone, with respect to the area in which Raman signal is available within the entire ring. In other words, it is also a comparison of a ring collection configuration with a conventional point collection configuration. In fact, if we consider an ideal homogeneous sample, for a given spatial offset Δs there is an entire circumference of points around the excitation area from which the Raman signal could theoretically be collected - corresponding to 2πΔs circumference. Since the collection area is of finite dimension, a ring should be considered rather than a circumference. For our specific parameters, micro-SORS theoretical ring collection area corresponds to only 1.067% (= 1/93.75) of the SORS ideal ring collection area, as depicted in Figure 3a. This means that, with an ideal ring collection geometry, SORS could collect signal from an area ~94 times larger than micro-SORS due to its ring area being larger. However, as our configuration is a point like and does collect signal from the entire ring, and since the spot collection area itself is still 93.75 smaller than that for SORS, overall our micro-SORS point collection geometry yields in absolute terms $93.75^2 \approx 9000$ times weaker signal than the SORS point collection geometry.

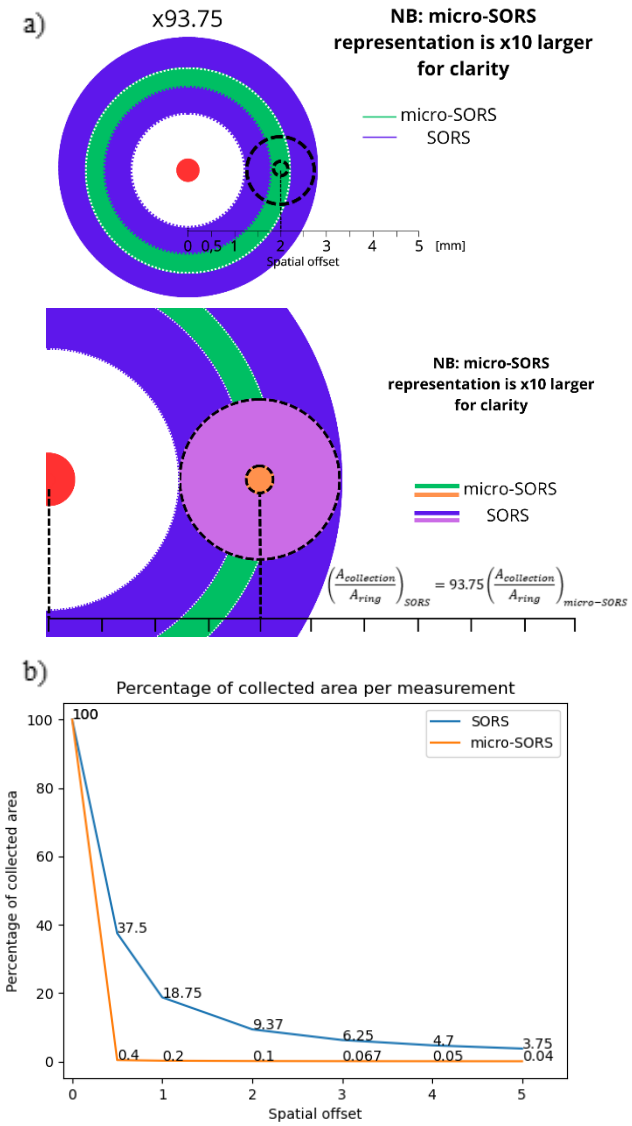

Figure 3. a) Schematics of theoretical collection rings of SORS and micro-SORS, and different collection disks between SORS and micro-SORS techniques; b) percentage of collected area (with respect to its theoretical ring collection) per measurement and at increasing offsets, considering the individual techniques. The amount of collected area for micro-SORS decreases much more rapidly.

Accordingly, SORS provides inherently stronger signals leading to higher signal-to-noise (S/N) ratios whereas micro-SORS configuration allows a sharper contrast between surface and offset spectra.

Schematics of the collected area by varying the spatial offset are shown in the Supporting Information (Figure S2 for SORS and S3 for micro-SORS).

Blurring of Spatial Offset Effect

Another consequence of large differences of the illumination and collection areas between SORS and micro-SORS is greater 'blurring' of spatial offsets in SORS measurements compared with micro-SORS ones. In our case, SORS has about 0.5 mm diameter excitation spot whereas micro-SORS only 0.028 mm diameter.

Assuming the excitation and collection spots were points, any portion of the laser spot would contribute to the signal at any given portion of the collection area with well-defined spatial offset, given by the separation of the two areas. However, when the illumination and collection areas are of finite sizes each imaginary point (P) within the collection zone would be receiving signals from multiple points within the illumination area of diverse spatial offsets. The overall signal would then be an integral of all contributions, each carrying its own spatial offset from a reference point (see Figure 4), yielding a composite Raman signal with a range of spatial offset contributing to it.

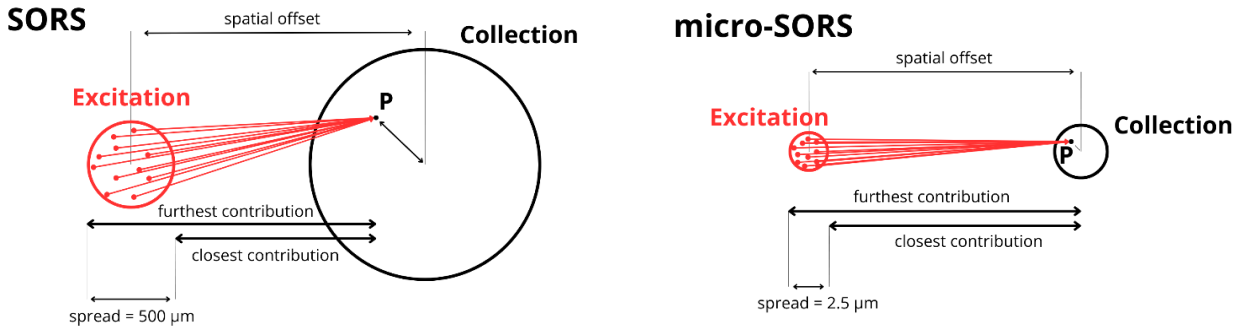

Figure 4. Schematics of the spread effect of the spatial offset for SORS (left) and micro-SORS (right). Notice that there are multiple points P within the collection area and this further blurs the spatial offsets 'seen' by the detection system.

The greatest offset of these contributions would be for the farthest away point from the reference point within the excitation zone, and the smallest would be the closest one, i.e. on the edge of the circle: on average, all points would render an effective spatial offset. Moreover, as there are multiple points P within the collection area this further blurs the spatial offsets 'seen' by the detection system.

However, the excitation and collection spots of micro-SORS are almost point-like with respect to SORS. This means that for a given spatial offset, SORS would carry a much greater spatial offset "spread" among the pairs of excitation and collection points – on the other hand, micro-SORS possesses excitation and collection areas much smaller leading typically to a reduced blurring effect and much better-defined magnitude of spatial offset for a given spatial offset.

A practical consequence of this phenomenon is reduction of signal contrast between layers in a stratified system.

Results and Discussion

Standard sample – S1

First, we measured a standard sample, polytetrafluoroethylene (PTFE) over polystyrene (PS) with reference spectra shown in Figure S5a. Multiple overlayer thicknesses were studied, namely 0.05, 0.1, 0.25, 0.5, 1, 2, 3, 4, 5 mm. The most representative results are given in Figure 5 and the rest are presented in the Supporting Information (Figs S6-11).

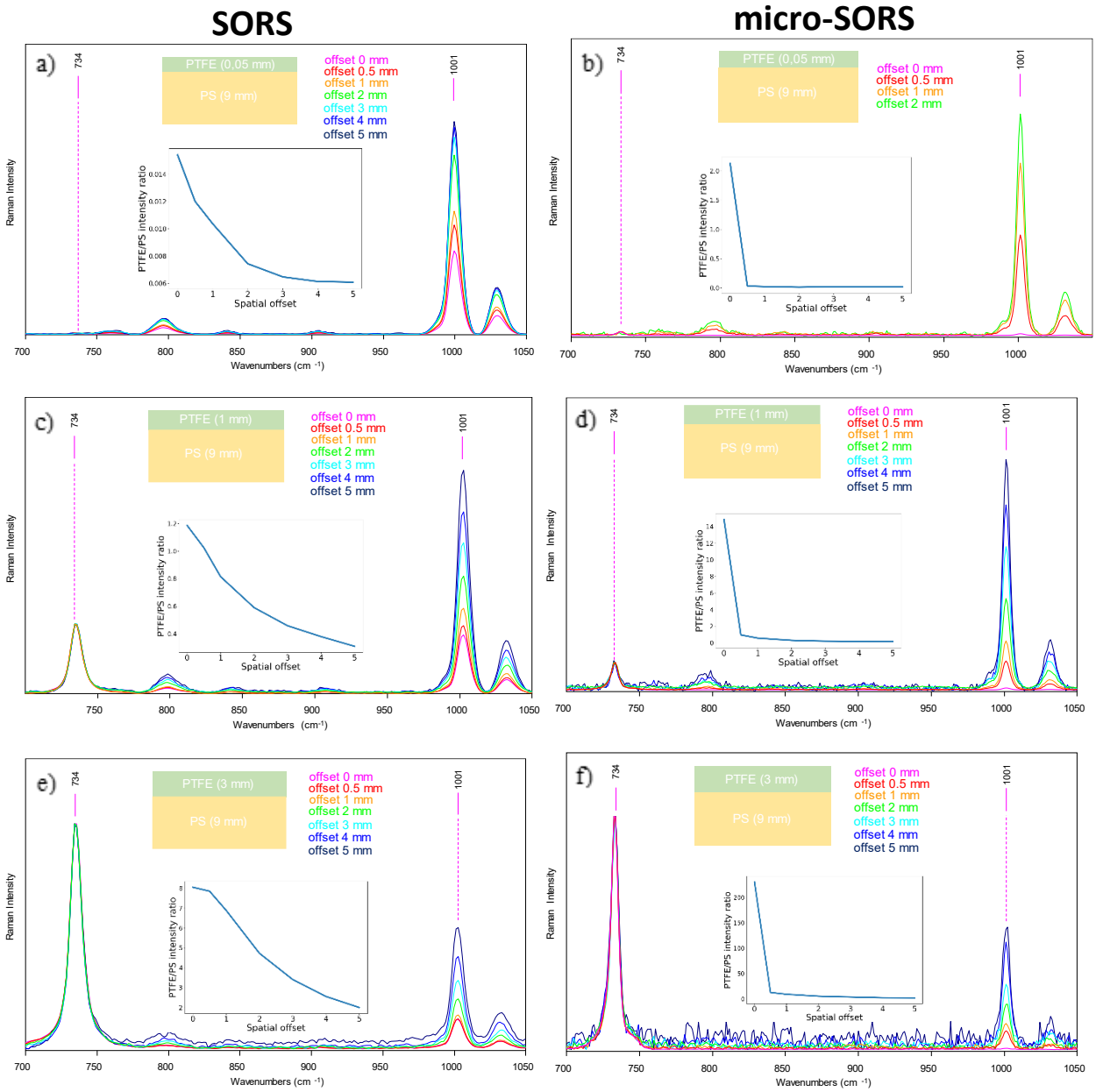

Figure 5. a) SORS and b) micro-SORS series of the standard sample (PTFE over PS) with 0,05 mm thick top layer. The inserts give intensity ratio versus spatial offset for each technique; c) SORS and d) micro-SORS series of the standard sample (PTFE over PS) with 1 mm thick top layer; e) SORS and f) micro-SORS series of the standard sample (PTFE over PS) with 3 mm thick top layer. All spectra have been normalized to the PTFE characteristic band at 734 cm^{-1}. The thinnest layers of PTFE were obtained by single or stacked layers of PTFE tape, which 50 µm thick.

An intuitive outcome can be immediately seen from Figure 5. As the thickness of the top layer increases, its band at 734 cm-1 naturally increases in intensity relative to the substrate signal at 1001 cm-1. In general, the greater the top layer thickness, the lower the signal from the bottom layer at any spatial offset for both SORS and micro-SORS. This also leads to lower signal-to-noise ratio as the top layer thickness increases, as already mentioned in the text and evident with 3 mm top layer thickness. The dependence of the top and bottom intensity ratios on the top layer thickness is more pronounced for the micro-SORS than SORS, as can be seen in the inset plots in Fig. 5 and SI; in fact, as a consequence of the smaller excitation and collection spot size, the signal from both top and bottom layers decreases much faster and so the influence of the top layer thickness is greater than for SORS. For example, at 0.05 mm top layer thickness, SORS struggles with seeing any top layer signal, whereas micro-SORS can detect it but only up to a certain spatial offset. Almost at any top layer thickness, micro-SORS sees a very weak bottom signal at 0 offset. The collection area effect is clearly visible: SORS has greater S/N ratio, thanks to its larger collection area. In turn, the intensity profiles of micro-SORS exhibit much more rapid decrease with increasing spatial offset due to larger contrast provided by this technique. In fact, the method is completely out of its typical regime regarding both the offsets and the top layer thicknesses, and this is also why in Figure 5b only spatial offsets up to 2 mm are shown spatial: beyond that step, the signal coming from the top layer was completely removed, rendering the normalization impossible. If we take a closer look at micro-SORS results with smaller spatial offset steps (Figure S12) it is possible to see the actual, smoother intensity profile present with micro-SORS too, even though still characterized by its sharper constrast between surface and offset spectra, due to the collection area effects explained above. It is also worth pointing out that the overlap effect has an influence on the outcome too, as SORS collects signal from the overlap area even at 1 mm spatial offset it provides a shallower decrease of the top layer signal, as demonstrated by the different intensity ratio profiles.

Painted stratigraphy – S2

After the standard sample, we analyzed realistic mock-up samples that mimic a painted stratigraphy. These were composed of red ochre and phthalocyanine blue as a two-layers system. Firstly, the thinnest top layer was considered, which was about 500 μm thick, and as shown in Figure S13a immediately a relevant issue appeared: even though the surface material was very thin, absorption of light in the employed wavelength range was so intense that no Raman signal from the substrate could be observed. Also the micro-SORS measurement (Figure S13b) showed the same results, even for smaller spatial offsets.

To check the above reasoning the surface material was substituted with a thicker PS layer (see Figure S5a for reference spectrum). As can be seen from Figure S14, when normalized to the polystyrene signal (1001 cm^{-1}), the signal of phthalocyanine blue (whose reference band is around 1529 cm^{-1}) clearly rises as the offset increases, indicating that our interpretation regarding the elevated absorption of the red ochre layer is correct.

It was evident that the results would not change with thicker red ochre top layers and so the samples with top layer thicknesses of 1-5 mm were discarded. Instead, lower thicknesses were selected to find out if any increase of the subsurface signal could be observed. It is intuitive to see that lowering of the top layer thickness means that the naturally micro-SORS regime is approached, and so a better performance (higher contrast) from this technique would be expected. The following spectra in Figure 6 show 0.3 and 0.15 mm

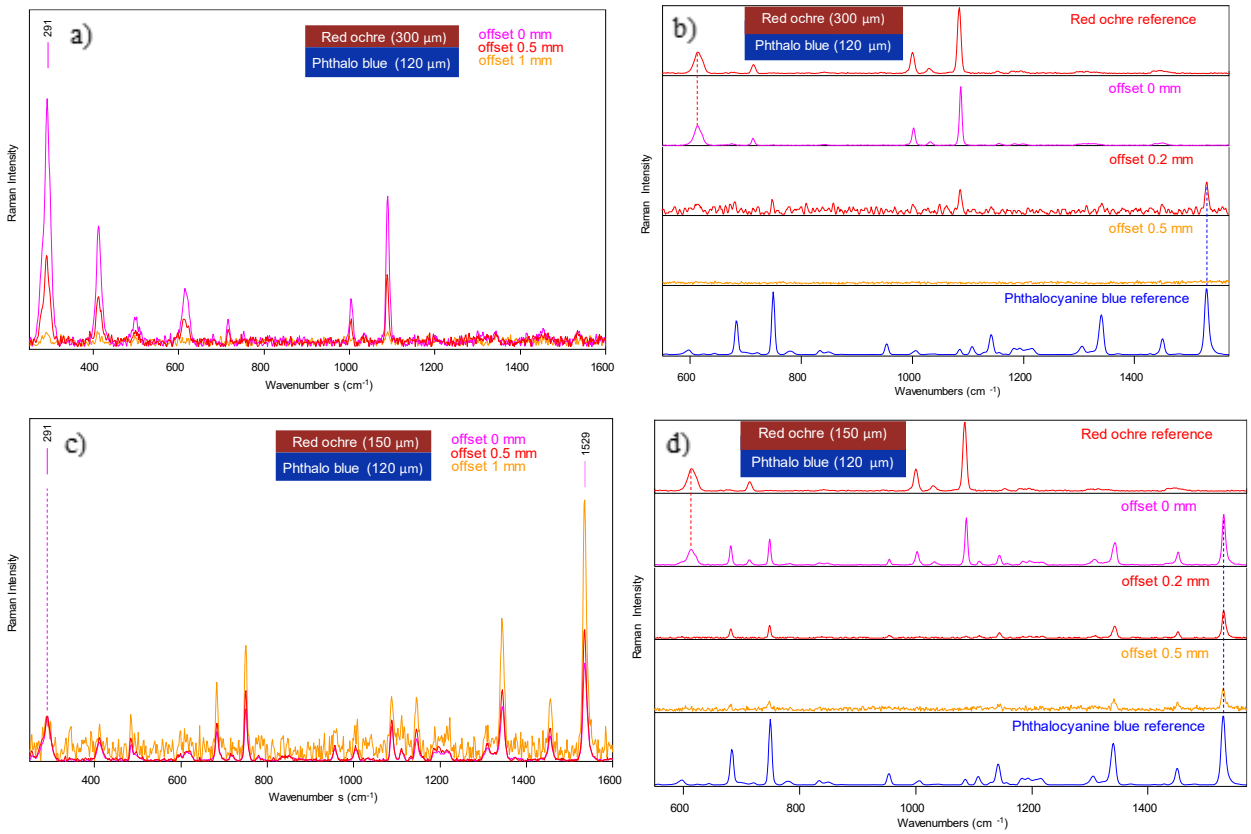

Figure 6. a) SORS and b) micro-SORS measurement of 300 µm red ochre (top layer) over 120 µm phthalocyanine blue substrate (bottom layer); c) SORS and d) micro-SORS measurement of 150 µm red ochre over 120 µm phthalocyanine blue substrate.

thick top layers (that is, 300 and 150 µm, respectively).

Once again, it is evident that the red ochre layer is highly absorptive with this wavelength: with 0.3 mm top layer thickness SORS is not able to detect the signal from the substrate, and micro-SORS loses any kind of signal already at 0.5 mm spatial offset. However, it is interesting to notice that micro-SORS is able to detect phthalocyanine blue signal at 0.2 mm spatial offset, meaning that there is an intermediary offset at which micro-SORS works better than SORS thanks to its higher contrast yielding capability (mostly given by the smaller overlap effect, and so the effective rejection for micro-SORS of the surface signal). Figure 6c,d show that with 0.15 mm thick top layer SORS is able to detect the rise of the substrate signal (i.e. phthalocyanine blue) but it is not as efficient as micro-SORS in removing the red ochre band from the surface: this is caused by the combination of the overlap and collection area effects. Overall, it appears that in case of painted stratigraphies involving red ochre as top layer, the latter has a limiting thickness beyond which it is not possible to probe the subsurface material. Below this limiting thickness (which would be around 300 µm),

micro-SORS provides great contrast between surface and subsurface signals, whereas SORS has lower resolution but would better deal with potential heterogeneity by greater averaging capability.

Limewash – S3

Limewash layers are usually made of calcium carbonate-based material or gypsum, and they are historically applied on murals or sculptures to preserve or cover them. These samples were designed to accurately mimic such layers. Gypsum layers of different thickness were selected for such purpose, and Carrara marble was chosen as substrate. Once again, the measurements started from the thinnest layer

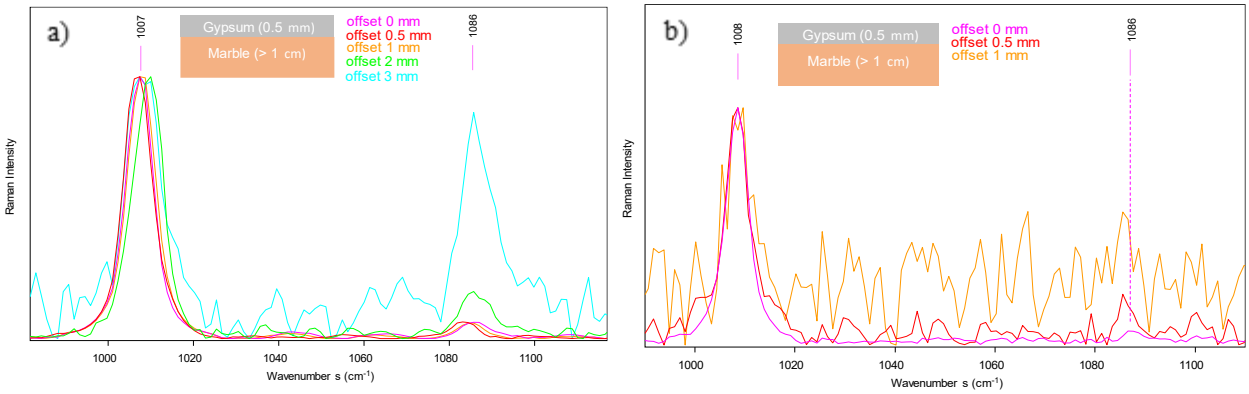

Figure 7. a) SORS series of thin gypsum layer over calcite substrate. The intensity rise of the calcite signal (1086 cm^{-1}) when normalizing to the gypsum band (1007 cm^{-1}) can be clearly seen; b) micro-SORS series of the same sample.

(about 0.5 mm thick).

Figure 7 shows SORS and micro-SORS series: by normalizing all the spectra to the gypsum signal (1007 cm^{-1}) an appreciable rise of the calcite signal (1086 cm^{-1}) can be observed as the offset increases, confirming a good SORS capability to retrieve the bottom layer signal when the overlayer has a low thickness. It is also possible to see another collection area effect in action: since SORS excites and collects signal from larger areas, it is able to detect Raman photons at larger offset than micro-SORS, and even though it may be an averaged signal it provides clean spectra with good S/N ratio, whereas micro-SORS spectra are very noisy already at 1 mm offset.

Nonetheless, SORS sensitivity to the bottom layer got considerably worse as its thickness was doubled: as it can be seen from Figure S15, detected calcite signal (bottom layer) is very low if not absent even with increasing the offset, possibly indicating great absorption from the gypsum layer (top layer). Naturally, as the thickness of the gypsum layer increased, its absorption rose as well, until the calcite signal could not be detected anymore.

In order to confirm this result, a highly scattering substrate was selected: a PTFE layer of about 9 mm thickness. As Figure S16 depicts, the trend is very similar to the previous result, meaning that an appreciable SORS effect can only be seen when the gypsum thickness is below or equal to 0.5 mm, indicating also in this case the presence of an upper limit of the overlayer thickness in the investigation of gypsum-based limewash layers.

Diffusion of salts inside stone – S4

This sample mimics salt diffusion inside a calcite matrix. Multiple spectra were collected in several locations with at zero spatial offset (corresponding to conventional Raman measurement) to confirm the homogeneity of the chemical composition of the top layer using the 2 mm thick layer from each composition. The results are shown in Figure S17, and they confirmed chemically homogeneous composition for all layers. However, these samples are heterogeneous in terms of thickness of the top layer that has an error of about 0.5 mm. Such sample was chosen on purpose to show the different behaviour of the SORS and micro-SORS methods when dealing with such type of heterogeneity. Outcomes are shown considering the different compositions. As before, here we present only representative spectra and the rest

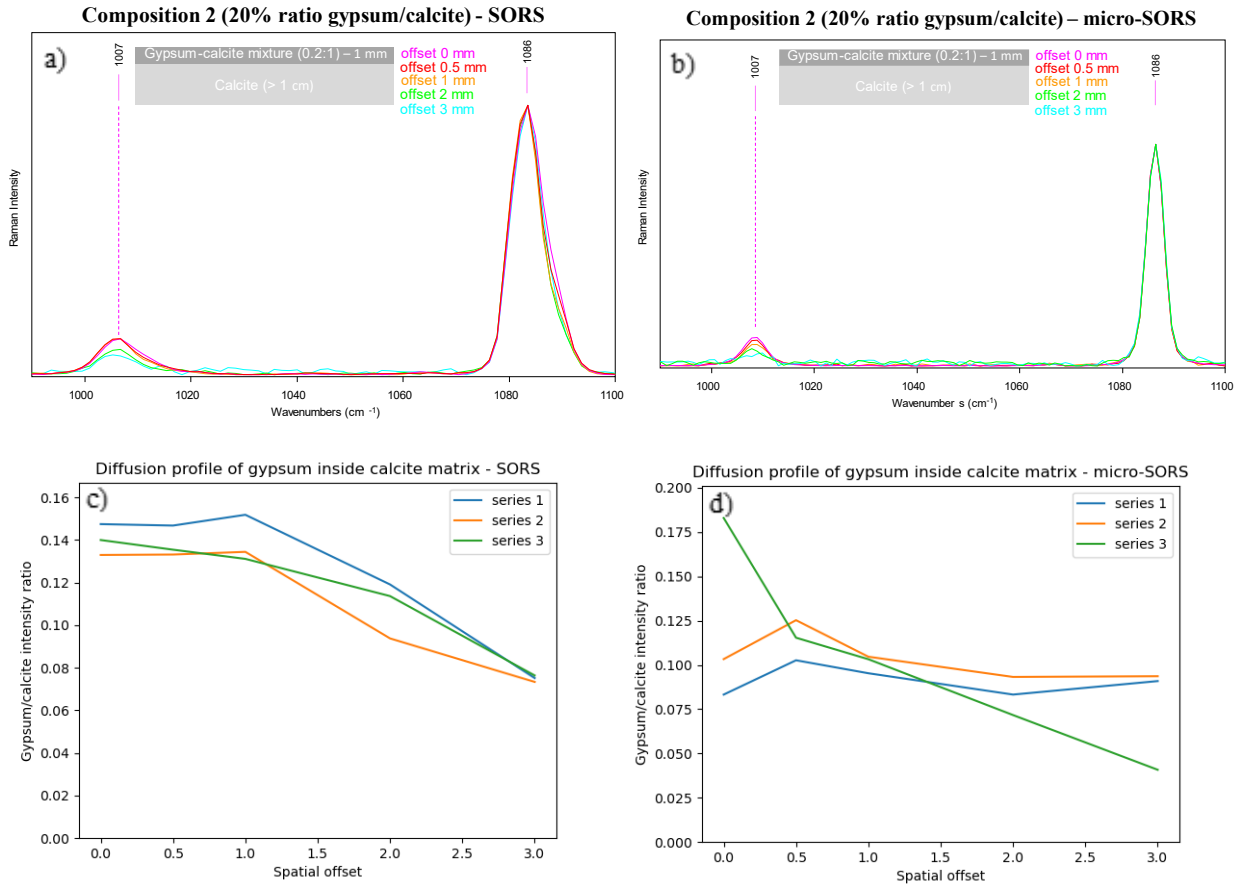

Figure 8. a) SORS and b) micro-SORS series of S4 sample (composition 2 – 20% of gypsum with respect to calcite in the top layer); c) SORS and d) micro-SORS intensity ratios of all the series collected on this sample.

are shown in the Supporting Information.

All the spectra were normalized to the calcite band (1086 cm^{-1}). The first notable observation is that the gypsum signal (1007 cm^{-1}) increases as its concentration in the top layer increases (see Figures 8 and S18,19). Moreover, it seems that the intensity of the gypsum signal in composition 1 (Figure S18) and 3 (Figure S19) does not diminish with spatial offset, indicating that the signal from the substrate was not detected. This is likely due to the optical properties (absorption and scattering) of the calcite-gypsum layer either preventing the laser photons from reaching the substrate or any potential Raman photons generated

from the sublayer from reaching the detector (as observed for the limewash sample, S3). Moreover, in composition 1 the lower amount of gypsum produced a less intense gypsum signal and consequently its detection with the increase of spatial offset was more challenging. These observations would indicate that there are optimum conditions that allow the probing of the diffusion of gypsum inside a calcite matrix. In fact, for completeness the thickness of the top layer was also doubled, but as was expected no improvement was obtained, since all compositions showed a constant gypsum signal when a 2 mm top layer was placed over the substrate within the error of the measurement and considering sample thickness variability.

There is another piece of information evident from Figure 8c,d related to sample heterogeneity and its reflection in the results of the two techniques: the spectral series collected with SORS is much more consistent with one another, whereas the spectra acquired with micro-SORS differ greatly from one another. This is explained by the vastly different excitation and collection area dimensions as discussed in the instrumental section. This renders micro-SORS more sensitive to local changes in sample heterogeneity (in this case the thickness of the top layer). This can either be a negative or positive aspect of the technique depending on the specific objective of the measurement.

Conclusions

We have compared SORS and micro-SORS techniques in order to shed more light on the diverse scenarios in which they can be applied, focusing on the borderline areas in which they could be both used as well as those were only one is favoured. Micro-SORS was applied to millimetric scale samples to test its potential and limitations. The aim was to create a systematic set of measurements that could help understand which method to employ and how best to interpret obtained data. The different settings give rise to multiple effects for which careful considerations are required: in particular, the overlap, the collection area and the spread of the spatial offset effects. We have shown how their combination renders SORS more suitable for highly heterogeneous samples where signal averaging is desirable. In case of homogeneous samples, the chosen method depends on the desired result: if higher contrast is required, micro-SORS is most suitable since it provides greater distinction between surface and substrate signals with more accurately defined spatial offsets, whereas if higher signal to noise ratio is necessary and the presence of top layer signal may be tolerated SORS would typically work better.

The higher spatial resolution of micro/SORS renders this technique suitable for imaging: in fact, it is possible to create chemical images of the surface and subsurface layers with a high degree of accuracy, highlighting the key differences between the inner and outer parts. However, as a consequence of the smaller spot size micro-SORS provides higher power density at the sample than SORS, and so potential damage can be induced. This could be relevant for many applications where even a small entity of such damage cannot be allowed, such as cultural heritage or biomedical fields: in these situations, precise tailoring of experimental parameters is required, and a compromise between satisfactory signal-to-noise ratio and high contrast between the top and bottom layers and spectral quality needs to be found. Nevertheless, the required intensities are not too dissimilar to those used routinely in conventional Raman microscopy.

Using representative samples in Cultural Heritage it has been demonstrated that micro-SORS is able to investigate effectively painted stratigraphies with increased detail, whereas SORS can better deal with heterogeneity evidenced when dealing with a compound diffusing into another. The application of these techniques is not limited to these circumstances and can vary depending on their different parameters: however, this study provides a generic practical guide aiding the understanding of their performance under different scenarios.

References

1. S. Mosca, C. Conti, N. Stone, P. Matousek. “Spatially offset Raman spectroscopy”. Nat. Rev. Methods Prim. 2021. 1(1): 21. 10.1038/s43586-021-00019-0.

2. P. Matousek, I.P. Clark, E.R.C. Draper, M.D. Morris, A.E. Goodship, N. Everall, et al. “Subsurface Probing in Diffusely Scattering Media Using Spatially Offset Raman Spectroscopy”. Appl. Spectrosc. 2005. 59(4): 393–400. 10.1366/0003702053641450.

3. P. Matousek, N. Everall, M. Towrie, A.W. Parker. “Depth profiling in diffusely scattering media using Raman spectroscopy and picosecond Kerr gating”,. Appl Spectrosc. 2005. 59: 200.

4. C. Conti, C. Colombo, M. Realini, G. Zerbi, P. Matousek. “Subsurface Raman Analysis of Thin Painted Layers”. Appl. Spectrosc. 2014. 68(6): 686–691. 10.1366/13-07376.

5. C. Conti, M. Realini, C. Colombo, K. Sowoidnich, N.K. Afseth, M. Bertasa, et al. “Noninvasive Analysis of Thin Turbid Layers Using Microscale Spatially Offset Raman Spectroscopy”. Anal. Chem. 2015. 87(11): 5810–5815. 10.1021/acs.analchem.5b01080.

6. A. Botteon, M. Vermeulen, L. Cristina, S. Bruni, P. Matousek, C. Miliani, et al. “Advanced Microspatially Offset Raman Spectroscopy for Noninvasive Imaging of Concealed Texts and Figures Using Raman Signal, Fluorescence Emission, and Overall Spectral Intensity”. Anal. Chem. American Chemical Society, 2024. 96(11): 4535–4543. 10.1021/acs.analchem.3c05249.

7. K. Chen, C. Massie, H.A. Awad, A.J. Berger. “Determination of best Raman spectroscopy spatial offsets for transcutaneous bone quality assessments in human hands”. Biomed. Opt. Express. 2021. 12(12): 7517. 10.1364/boe.440297.

8. S. Mosca, P. Dey, M. Salimi, B. Gardner, F. Palombo, N. Stone, et al. “Spatially Offset Raman Spectroscopy - How Deep?” Anal. Chem. 2021. 93(17): 6755–6762. 10.1021/acs.analchem.1c00490.

9. P. Dey, A. Vaideanu, S. Mosca, M. Salimi, B. Gardner, F. Palombo, et al. “Surface enhanced

deep Raman detection of cancer tumour through 71 mm of heterogeneous tissue". Nanotheranostics. Ivyspring International Publisher, 2022. 6(3): 337–349. 10.7150/ntno.71510.

10. S. Mosca, P. Dey, M. Salimi, F. Palombo, N. Stone, P. Matousek. "Non-invasive depth determination of inclusion in biological tissues using spatially offset Raman spectroscopy with external calibration". Analyst. Royal Society of Chemistry, 2020. 145(23): 7623–7629. 10.1039/D0AN01292K.

11. P. Strobbia, V. Cupil-Garcia, B.M. Crawford, A.M. Fales, T.J. Pfefer, Y. Liu, et al. "Accurate in vivo tumor detection using plasmonic-enhanced shifted-excitation Raman difference spectroscopy (SERDS)". Theranostics. 2021. 11(9): 4090–4102. 10.7150/thno.53101.

12. D.I. Ellis, R. Eccles, Y. Xu, J. Griffen, H. Muhamadali, P. Matousek, et al. "Through-container, extremely low concentration detection of multiple chemical markers of counterfeit alcohol using a handheld SORS device". Sci. Rep. 2017. 7(1): 12082. 10.1038/s41598-017-12263-0.

13. K. Shin, H. Chung. Wide area coverage Raman spectroscopy for reliable quantitative analysis and its applications. Analyst. 2013. 10.1039/c3an36843b.

14. A. Botteon, W.-H. Kim, C. Colombo, M. Realini, C. Castiglioni, P. Matousek, et al. "Non-destructive Monitoring of Dye Depth Profile in Mesoporous TiO 2 Electrodes of Solar Cells with Micro-SORS". Anal. Chem. 2022. 94(6): 2966–2972. 10.1021/acs.analchem.1c05011.

15. S. Mosca, K. Sowoidnich, M. Mehta, W.H. Skinner, B. Gardner, F. Palombo, et al. "10 kHz Shifted-Excitation Raman Difference Spectroscopy with Charge-Shifting Charge-Coupled Device Read-Out for Effective Mitigation of Dynamic Interfering Backgrounds". Appl. Spectrosc. SAGE Publications Ltd STM, 2023. 77(6): 569–582. 10.1177/00037028231167441.

16. "Mathworld". n.d.

17. M.A. Green, M.J. Keevers. "Optical properties of intrinsic silicon at 300 K". Prog. Photovoltaics Res. Appl. 1995. 3(3): 189–192. 10.1002/pip.4670030303.

18. M.A. Green. "Self-consistent optical parameters of intrinsic silicon at 300K including temperature coefficients". Sol. Energy Mater. Sol. Cells. 2008. 92(11): 1305–1310. 10.1016/j.solmat.2008.06.009.